11. Geodynamics

Experiment MA-128

F. O. Vonbun,[a†] W. D. Kahn,[a] W. T. Wells,[b] and T. D. Conrad[b]

ABSTRACT

The Apollo-Soyuz Test Project Geodynamics Experiment was performed to assess the feasibility of tracking and recovering high-frequency components of the Earth gravity field by utilizing a synchronous orbiting tracking station such as Applications Technology Satellite 6. Gravity anomalies of 0.05 mm/sec^2 (5 mgal) or larger having wavelengths of 300 to 1000 km on the surface of the Earth are important for geologic studies of the upper layers of the Earth crust. Two prime areas of data collection were selected for this experiment: the center of the African Continent and the Indian Ocean Depression centered at latitude 5° N and longitude 75° E.

Results show that the detectability objective of the experiment was achieved in both areas as well as in several additional anomalous areas around the globe. Gravity anomalies of the Karakoram and Himalayan mountain ranges, of ocean trenches, and of the Diamantina Depth are specific examples.

The more complicated aspect of the experiment was that of recovering the magnitude of the gravity field perturbations that produced the signatures in the experiment data residuals. Recovery of discretely distributed gravity anomalies has been successfully accomplished for the prime area; i.e., the Indian Ocean Depression. Residual patterns over other geographic areas also indicate possible gravity anomalies, which are the subject for further investigation.

Comparisons of values of the recovered gravity anomalies with surface gravity measurements (ground truth) are generally in good agreement. It is estimated that the accuracy of the recovered anomalies is approximately $\pm$ 0.10 mm/sec^2 ($\pm$ 10 mgal) or better.

INTRODUCTION

The objectives of the Apollo-Soyuz Test Project (ASTP) Geodynamics Experiment were threefold.

1. To demonstrate the detectability of short-wavelength (i.e., 300 km and larger) features of the Earth gravity field
2. To evaluate the "high/low" satellite-to-satellite tracking (SST) concept for geodynamics applications
3. To test the recoverability of short-wavelength features of the Earth gravity field

This experiment was the culmination of an effort to utilize synchronous orbiting tracking stations for NASA missions (ref. 11-1). The use of a

[a]NASA Goddard Space Flight Center.

[b]Washington Analytical Services Center, Inc., Riverdale, Maryland.

[†]Principal Investigator.

low-orbiting (approximately 230 km) spacecraft, such as Apollo-Soyuz, continuously tracked by a synchronous satellite has, for the first time, led to the detection of short-wavelength Earth gravity anomalies (ref. 11-2).

The Apollo-Soyuz spacecraft, flying in a low orbit, is particularly sensitive to gravity anomalies. For example, the ratio of sensitivity to the 25th-degree terms of the Earth gravity potential having a wavelength of approximately 1600 km is approximately 13 to 1 when going from a Geodetic Earth Orbiting Satellite 3 (GEOS-3) type orbit (840 km) to the lower Apollo orbit (223 km). Thus, the ASTP mission presented an excellent opportunity to test the SST concept. Normal satellite perturbation methods used previously for computing the Earth gravity field cannot be used for such short wavelengths because this would require a spherical harmonic expansion to an order and degree of 120 or larger.

During the course of the ASTP mission, MA-128 experiment data were collected for 108 revolutions; 28 revolutions were originally scheduled for the experiment and the remaining 80 revolutions were targets of opportunity. In all the experiment revolutions analyzed, it has consistently been shown that gravity field signatures in the 500- to 1000-km-range wavelengths manifested themselves on the experiment data residuals. The more complicated problem of recovering the magnitude of the gravity anomalies producing the aforementioned perturbations will now be considered.

MATHEMATICAL METHODS

The gravitational field of the Earth is generally represented in terms of a finite spherical harmonic series expansion having coefficients determined from a combination of satellite ground tracking data and surface gravimetric data. Such a limited representation of the global geopotential does not adequately "model" local variations in the gravity field because the short wavelengths of these local variations would require a field expansion to a degree and order of approximately 100 to 200. This is considered impractical if not impossible. However, rather small local gravity anomalies are important for geologic investigations of the upper crust as well as for studies of the ocean topography. This experiment provided an opportunity to improve knowledge of the terrestrial gravitational field in localized areas by directly measuring local gravity variations through detection of small velocity changes (1 to 10 mm/sec) of the low-orbiting spacecraft. Before the gravity anomaly analyses are discussed, some basic information about the tracking system will be presented. Figure 11-1 is a schematic of the Applications Technology Satellite 6 (ATS-6)/Apollo communication links. The Apollo spacecraft was connected with Madrid by two links: the ATS-6 link and a direct ground link. This provides a total loop for the measurements that will be used to reduce the errors in the system. The emphasis in this report is on the link from Madrid to ATS-6 to Apollo and back. Figure 11-2 depicts the range rates that were actually measured during the experiment. The system was constructed to measure the total range rate between the ground station (in this case Madrid) and the Apollo spacecraft in Earth orbit. The total range rate is the sum of the range rates between Madrid and ATS-6 $\dot{r}_1$, ATS-6 and Apollo $\dot{r}_2$, Apollo and ATS-6 $\dot{r}_3$, and ATS-6 and Madrid $\dot{r}_4$ (ref. 11-3). This analysis concentrates only on variations of the range rate between Apollo and ATS-6 $\dot{\rho}_A$, which is a dot product of the spacecraft velocity vector $\mathbf{v}$ and the unit vector between Apollo and ATS-6 $\dot{\rho}^0$ as seen in figure 11-2.

$$\dot{\rho}_A = \rho^0 \cdot \mathbf{v} \qquad (11\text{-}1)$$

One of the first experiment tasks was to evaluate the noise characteristics of the total system. An analysis performed before the experiment was the basis for a predicted range-rate noise level of approximately 0.05 cm/sec using a 10-second integration time (fig. 11-3). The actual experimental

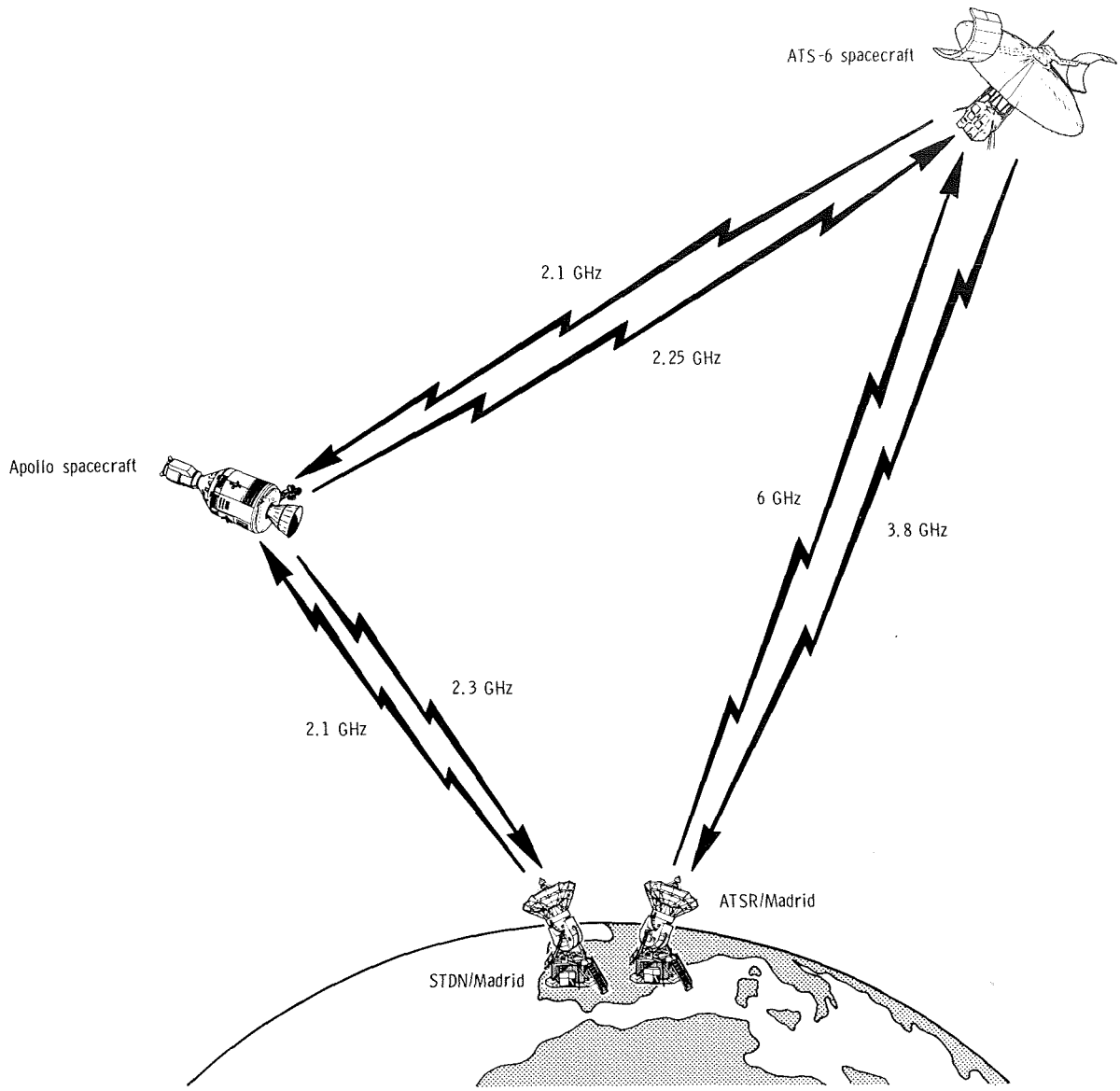

FIGURE 11-1.—Schematic of the ATS-6/Apollo communication links for operations with ATS-6 in the Eastern Hemisphere. The ATS ranging station is designated ATSR; the Spaceflight Tracking and Data Network station is designated STDN.

range-rate noise level, approximately 0.03 cm/sec, was lower than predicted. These values were obtained using a small portion of an orbit to minimize possible orbit modeling errors. These noise values have been rather consistent throughout all the experimental arcs analyzed.

Two approaches were taken to test the detectability of gravity anomalies. The first approach consisted of assuming a single mass anomaly Δm and of computing, in a simple analytical manner, the expected variation of the spacecraft velocity Δv due to this anomaly (ref. 11-2). The velocity

variations in the radial and horizontal components, respectively, are then

$$\Delta v_{\rho} = -\frac{\Delta m}{m} v_{horiz} \left\{ \frac{1+x}{2(1-x)^2} \frac{\Delta\theta}{\sqrt{1 + \frac{x}{(1-x)^2}\Delta\theta^2}} + \frac{1}{2\sqrt{x}} \ln\left[\frac{\sqrt{x}}{1-x}\Delta\theta + \sqrt{1 + \frac{x}{(1-x)^2}\Delta\theta^2} \right] \right\} \quad \text{(11-2a)}$$

$$\Delta v_{\theta} = v_{horiz} \frac{\Delta m}{m} \left(\frac{1}{\sqrt{1 + x^2 - 2x\cos\Delta\theta}} - 1 \right) \quad \text{(11-2b)}$$

where $x = \frac{R-d}{R+H}$

$\Delta\theta = vt$

$t \approx 0$ to 150 seconds

R = radius of the Earth

d = anomaly depth

H = satellite altitude

Equations (11-2a) and (11-2b) assume that the spacecraft travels directly over the anomaly and are only valid for variations in true anomaly of as much as ± 5°, which corresponds to approximately 1.5 minutes of flight time. The dashed curve in figure 11-4 represents the radial velocity variation due to a 0.05 mm/sec^2 (5-mgal) anomaly (4° by 4°). The size of the anomaly block is roughly twice the orbital height and represents the area of sensitivity of a spacecraft in orbit to an anomaly on the ground (ref. 11-4). Because of the extremely low noise in the data and the actual geometry (i.e., the spacecraft was not directly over the mass and it was an extended mass rather than a point mass), a second approach, using computer simulation techniques, was necessary to improve the analytical results.

The dotted line in figure 11-4 depicts the result of the computerized analysis. As shown in figure 11-2, the value $\dot{\rho}$ is defined as (ref. 11-5)

$$\dot{\rho} = \dot{r}_1 + \dot{r}_2 + \dot{r}_3 + \dot{r}_4 \quad \text{(11-3)}$$

This is the range rate as actually measured at the Madrid Applications Technology Satellite Ranging (ATSR) station. However, only the range rate between the Apollo spacecraft and the ATS-6 spacecraft $\dot{\rho}_A$, which is the dot product of the spacecraft orbital velocity vector $\mathbf{v}$ and the unit vector ρ^0 between Apollo and ATS-6, is of interest (eq. (11-1)). The ATS-6 orbit is almost independent of any gravity variations because of its extreme height (36 000 km); therefore, the range rate between ATS-6 and Madrid can simply be subtracted from the measured range rate. That is,

$$\dot{\rho}_A \approx \dot{\rho} - \dot{\rho}(\text{ATS-6/Madrid}) \quad \text{(11-4)}$$

which reduces to 1, the quantity needed for further analyses. This range rate is, however, a function of the state vectors and the gravity field.

$$\dot{\rho}_A = f\left(X_A, X_{ATS}, G\right) \quad \text{(11-5)}$$

where X_A and X_{ATS} are the Apollo and ATS-6 state vectors, respectively, and G represents the gravity field. The major aim in this experiment was to determine the relationship between surface gravity anomalies Δg and the Apollo/ATS-6 range-rate variations $\Delta\dot{\rho}_A$. Again, because only

the variation in $\dot{\rho}_A$ is of interest, equation (11-5) is varied as follows.

$$\Delta\dot{\rho}_A \approx \frac{\partial f}{\partial X_A}\left(\frac{\partial X_A}{\partial X_A^0}\right)\Delta X_A^0 + \frac{\partial f}{\partial X_{ATS}}\left(\frac{\partial X_{ATS}}{\partial X_{ATS}^0}\right)\Delta X_{ATS}^0 + \frac{\partial f}{\partial X_A}\left(\frac{\partial X_A}{\partial G}\right)\Delta G \qquad (11\text{-}6)$$

Also

$$\Delta\dot{\rho}_A \approx \left(\Delta \mathbf{v}_\theta + \Delta \mathbf{v}_\rho\right)\cdot\boldsymbol{\rho}^0$$

is equal to the observed-computed range rate.

The sensitivity coefficient $(\partial X_A/\partial G)$ is now contained in equation (11-6) together with ΔG, and thus relates the actual measurements with the gravity potential variation ΔG. Because local

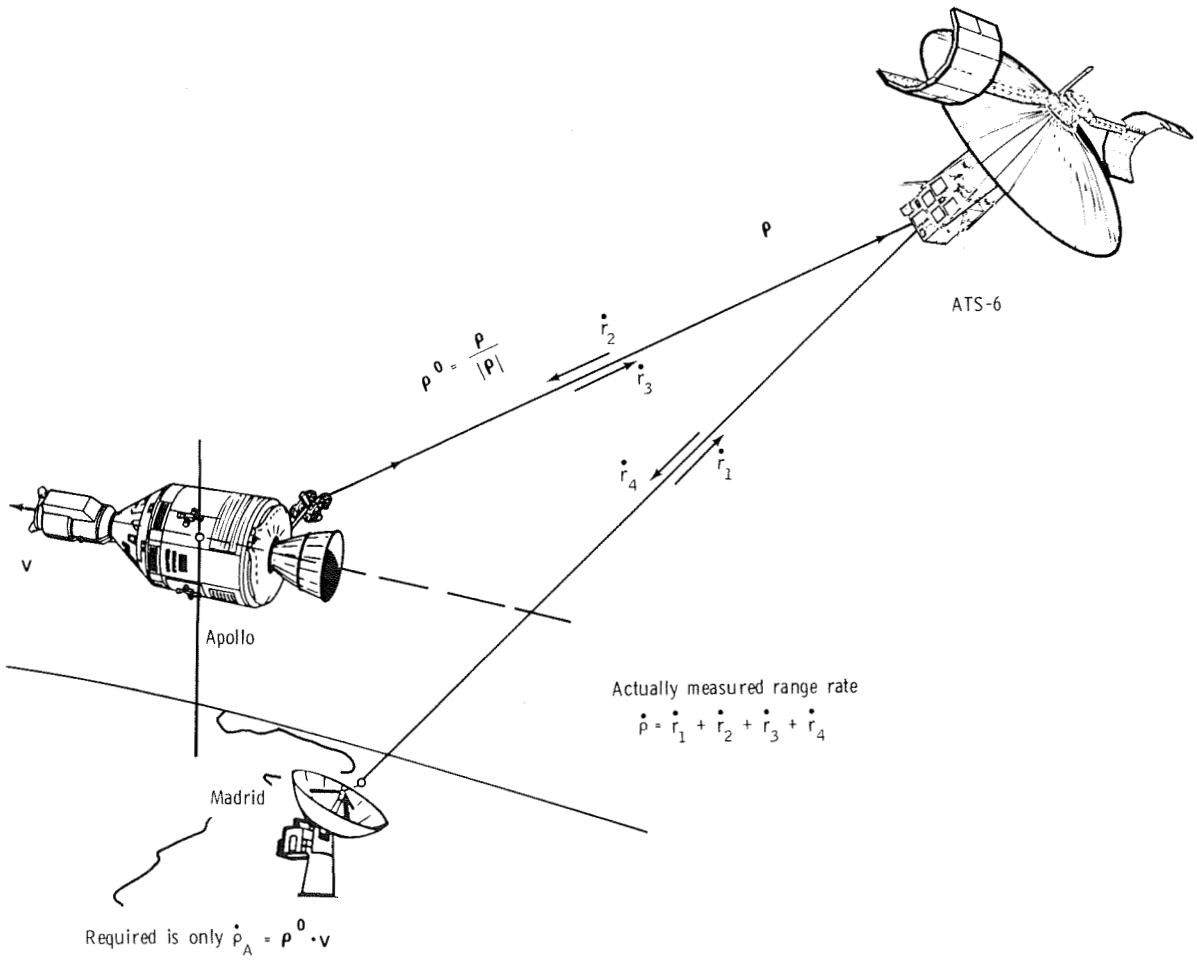

FIGURE 11-2.—Schematic showing range-rate measurement for the ATS-6 and Apollo vehicles.

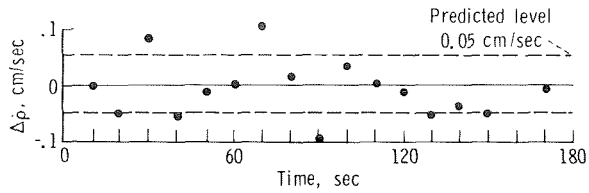

FIGURE 11-3.—Tracking systems range-rate noise characteristics measured from Madrid to ATS-6 to Apollo-Soyuz to ATS-6 to Madrid.

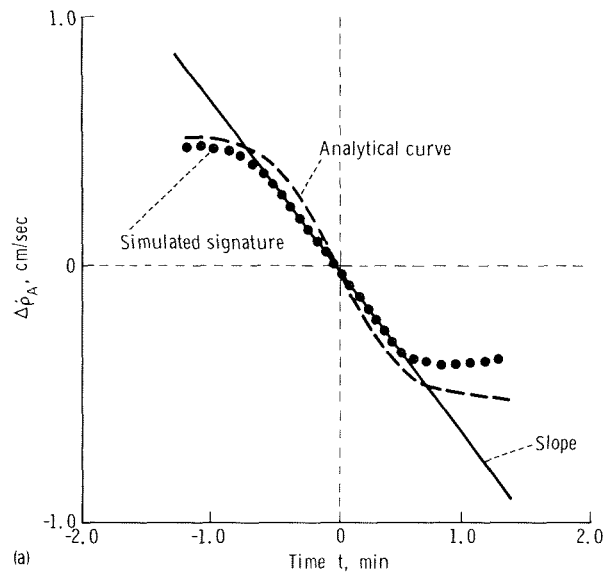

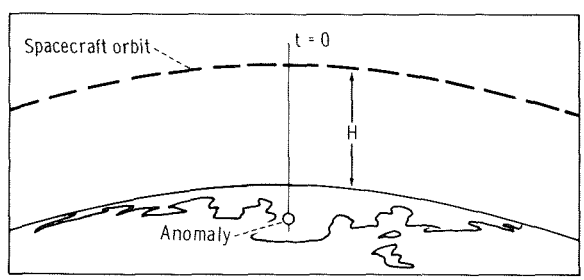

FIGURE 11-4.—Analytical and computer-simulated range-rate signature for a 4° by 4°, 0.05 mm/sec^2 (5-mgal) anomaly. (a) Plot. (b) Schematic.

anomalies are being observed over a very brief time (as seen in fig. 11-2, approximately a few minutes), the first two terms on the right side of the series expansion can be neglected. Thus, equation (11-6) reduces to

$$\Delta\dot{\rho}_A \approx \frac{\partial f}{\partial X_A}\left(\frac{\partial X_A}{\partial G}\right)\Delta G \tag{11-7}$$

This sensitivity coefficient can now be computed using Newton's equation of planetary motion.

$$\ddot{X}_A = \frac{\partial V}{\partial X_A} = F\left(X_A, G\right) \tag{11-8}$$

Differentiating equation (11-8) with respect to G yields

$$\frac{\partial \ddot{X}_A}{\partial G} = \frac{\partial F}{\partial X_A}\left(\frac{\partial X_A}{\partial G}\right) + \frac{\partial F}{\partial G} \tag{11-9}$$

Because $(\partial X_A/\partial G)$ is the variable to be determined, equation (11-9) can be rewritten in the following manner, assuming interchangeability of differential operators; that is

$$\frac{\partial \ddot{X}_A}{\partial G} = \frac{d^2}{dt^2}\left(\frac{\partial X_A}{\partial G}\right) = \frac{\partial}{\partial X_A}\left(\frac{\partial V}{\partial X_A}\right)\left(\frac{\partial X_A}{\partial G}\right) + \frac{\partial}{\partial G}\left(\frac{\partial V}{\partial X_A}\right) \tag{11-10}$$

where $V = U + T$

U = the normal potential of the Earth gravity field in spherical harmonics

$T = \frac{R}{4\pi} \iint_{\sigma} \Delta g S(\psi)\, d\sigma$

$\Delta g = \Delta G + \Delta g_{LOC}$ using Δg_{LOC} as the local average anomaly of a block (4° by 4°, as an example)

T = the disturbing potential due to the anomalies Δg

R = the radius of a sphere having a volume equal to that of the spheroid

$S(\psi)$ = the Stokes function

σ = an element of surface area

Introducing U and T into equation (11-10) yields

$$\frac{d^2}{dt^2}\left(\frac{\partial X_A}{\partial G}\right) = 2\frac{\partial^2}{\partial X_A}(U + T)\left(\frac{\partial X_A}{\partial G}\right) + \frac{\partial^2}{\partial X_A \partial G}(U + T) \tag{11-11}$$

Equation (11-11) is now solved for the sensitivity coefficient ($\partial X_A / \partial G$) by numerical integration. Using equation (11-7), the computed sensitivity coefficient is correlated and the relationship between $\Delta \dot{\rho}_A$ and ΔG is established. The following procedures were used in detecting the gravity anomalies.

An orbit of one to one and one-half revolutions was computed for the Apollo spacecraft using the Goddard Earth Model 1 (GEM-1) (ref. 11-6) gravity field and all available tracking data (ground station as well as SST). From these Apollo orbits, together with the ATS-6 orbit, the range rates $\dot{\rho}_A$ between ATS-6 and Apollo were computed. These computed range rates were subtracted from the actual measured ones to yield the $\Delta \dot{\rho}_A$ shown in figures 11-5 and 11-6. These values of $\Delta \dot{\rho}_A$ are finite rather than zero because the gravity field, which would necessarily include all the gravity anomalies, is not known to a very high accuracy. To obtain more precise knowledge of the gravity field, of course, is the essence of this experiment.

DETECTABILITY

Experimental data were collected in the Eastern Hemisphere region where the Apollo-Soyuz spacecraft was in range of the ATS-6 satellite (which was positioned over the Equator at approximately longitude 35° E). The duration of each Apollo orbit visible to ATS-6 was approximately 50 minutes, or slightly greater than one-half an orbital revolution. To eliminate occultation effect (appendix A), the actual SST data passes used were limited to approximately 40 minutes. All data were successfully collected using the ATS-6 spacecraft and the Madrid ATSR station as the prime ground station. Preliminary results confirm that the range-rate noise of 0.05 cm/sec, computed before the experiment, was improved by the experimental data, which show an average noise of approximately 0.03 cm/sec (fig. 11-3). Figure 11-7 shows the groundtrack of Apollo revolution 115, which coincidentally passed over anomalies in the African area. The effect of the anomalies is apparent in the residual plot.

Figure 11-8 shows three orbital passes (revolutions 8, 23, and 53) that passed over both the Indian Ocean Depression and the Himalayan mountain range. Figures 11-5 and 11-6 depict the actual measurement residuals obtained; that is, the observed minus the computed values. The Indian Ocean Depression can be "seen" in the actual data. The shape of the range-rate variations from the Indian Ocean Depression actually fits the expected shape computed in a manner similar to those shown in figure 11-4. Detectability of the gravity field perturbations has thus been demonstrated to be manifested in the expected form of

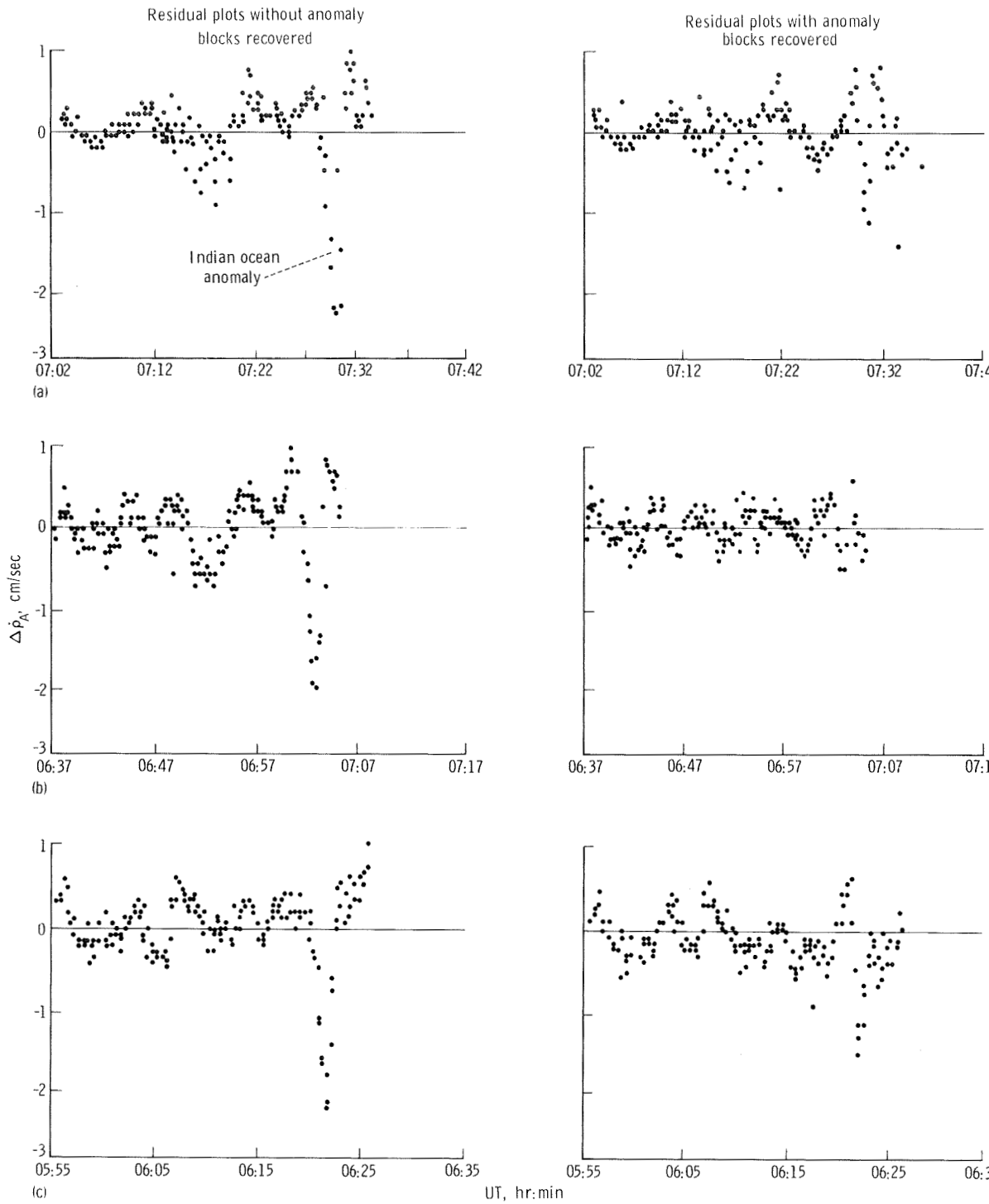

FIGURE 11-5.—Residual plots for ascending revolutions 8, 23, and 53 both with and without anomaly blocks recovered. The GEM-1 reference gravity field model was used. (a) Revolution 8, July 16, 1975. (b) Revolution 23, July 17, 1975. (c) Revolution 53, July 19, 1975.

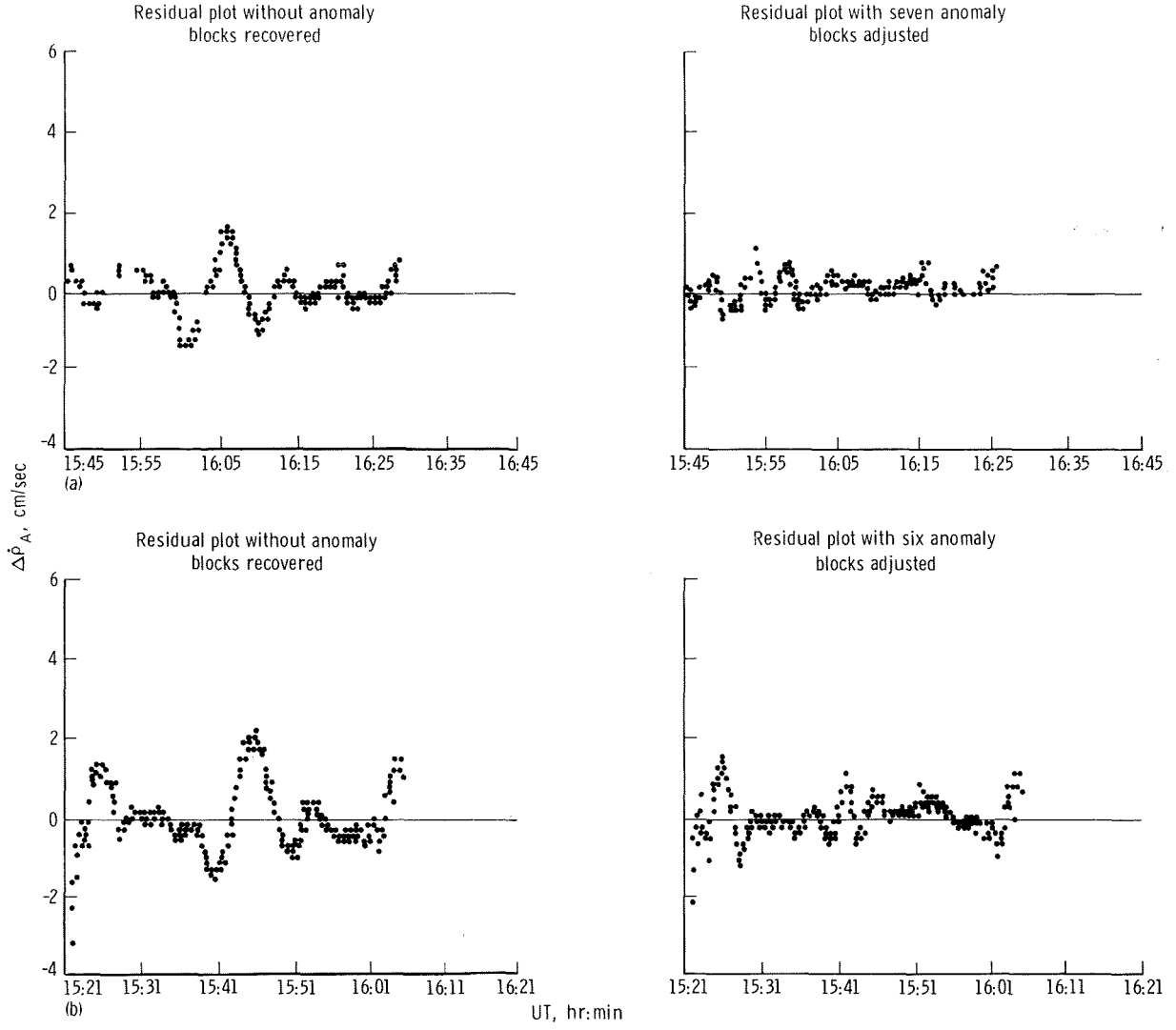

FIGURE 11-6.—Residual plots for descending revolutions 120 and 135 both with and without anomaly blocks recovered. The GEM-1 reference gravity field model was used. (a) Revolution 120, July 23, 1975. (b) Revolution 135, July 24, 1975.

small velocity variations of the spacecraft. The peak values of these variations could, in most cases, be closely correlated with anomalies shown on the detailed map of the global geoid. Other features may have been detected but cannot be verified at this time because of a lack of surface gravimetric data in these areas, particularly in the southern portion of the globe. It may be assumed, however, that the detected gravity signatures in the southern part of the Earth represent existing anomalies that are not well known.

Orbit determination required for the proper analysis of the experimental data involves the use of SST range-rate data together with direct ATS-6 tracking data and unified S-band tracking data. The error analysis performed indicates that one- and two-revolution arcs are superior for minimizing the effects of unmodeled error in the detection and recovery of gravity anomalies.

Longer arcs seem to introduce larger errors because the influence of the Earth gravity field errors on the orbit errors becomes more pronounced as the arc length increases. Shorter arcs, however, also have rather large errors because not enough tracking data are available. Thus, the use of one- to two- orbit revolutions for the analyses seems to be a good optimum. Air-drag corrections have been used for Apollo-Soyuz orbit determination. The SST data were used only during those periods judged free of onboard propulsion activities. Because the antenna is separated from the spacecraft axis by approximately 3 m, any attitude motion (correction) of the spacecraft (rotation of the spacecraft) is transformed into a range rate between the Apollo-Soyuz spacecraft and the ATS-6 spacecraft. One could therefore quite wrongly interpret a spacecraft rotation as a gravity anomaly. Detailed analysis of attitude control has not yet been performed; however, attitude data are available and will be used to further refine the range-rate residuals measured between the Apollo-Soyuz and ATS-6 vehicles. The SST data were corrected for ionospheric effects before processing.[1]

RECOVERY OF GRAVITY ANOMALIES

Groundtracks of some of the ASTP MA-128 experiment revolutions analyzed for gravity anomaly recovery are shown in figure 11-8. Note the center of the prime experiment region, i.e., the Indian Ocean Depression, is represented by block C. Another geographic feature that can be correlated with large variations in the residual signature is in the boundary region between the Eurasian

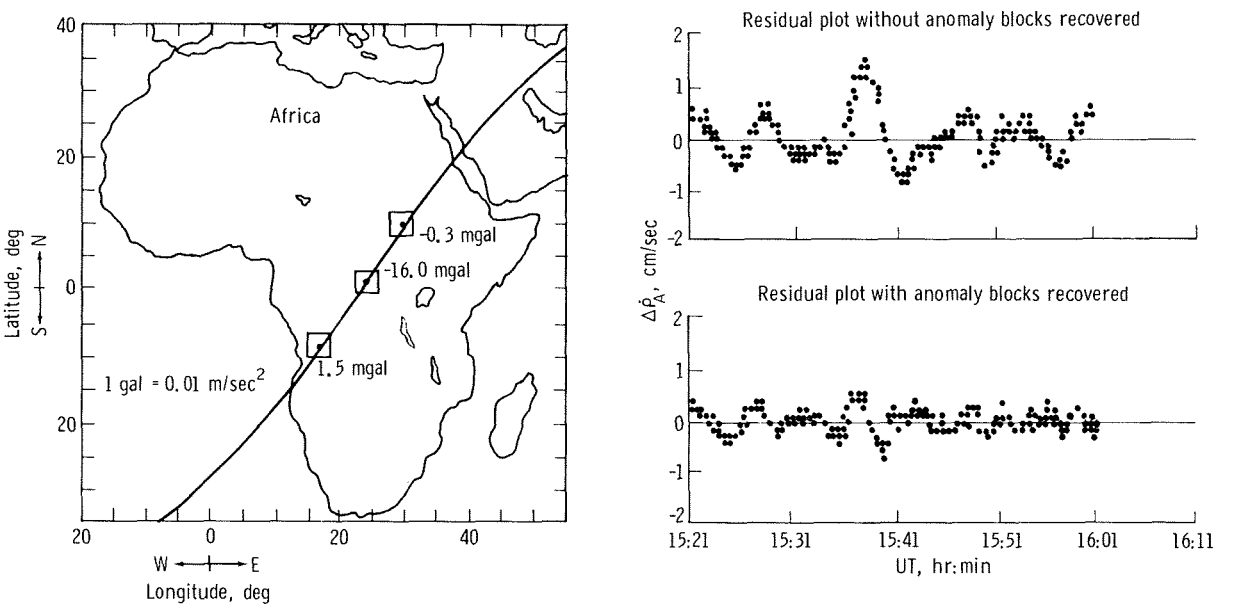

FIGURE 11-7.—Groundtrack and residual plot for revolution 115, July 24, 1975. Recovered value for 4° by 4° anomaly blocks is indicated along the trajectory.

[1]Ionospheric corrections applied to these data were supplied by R. B. Bent, Atlantic Science Corp., Melbourne, Florida (private communication).

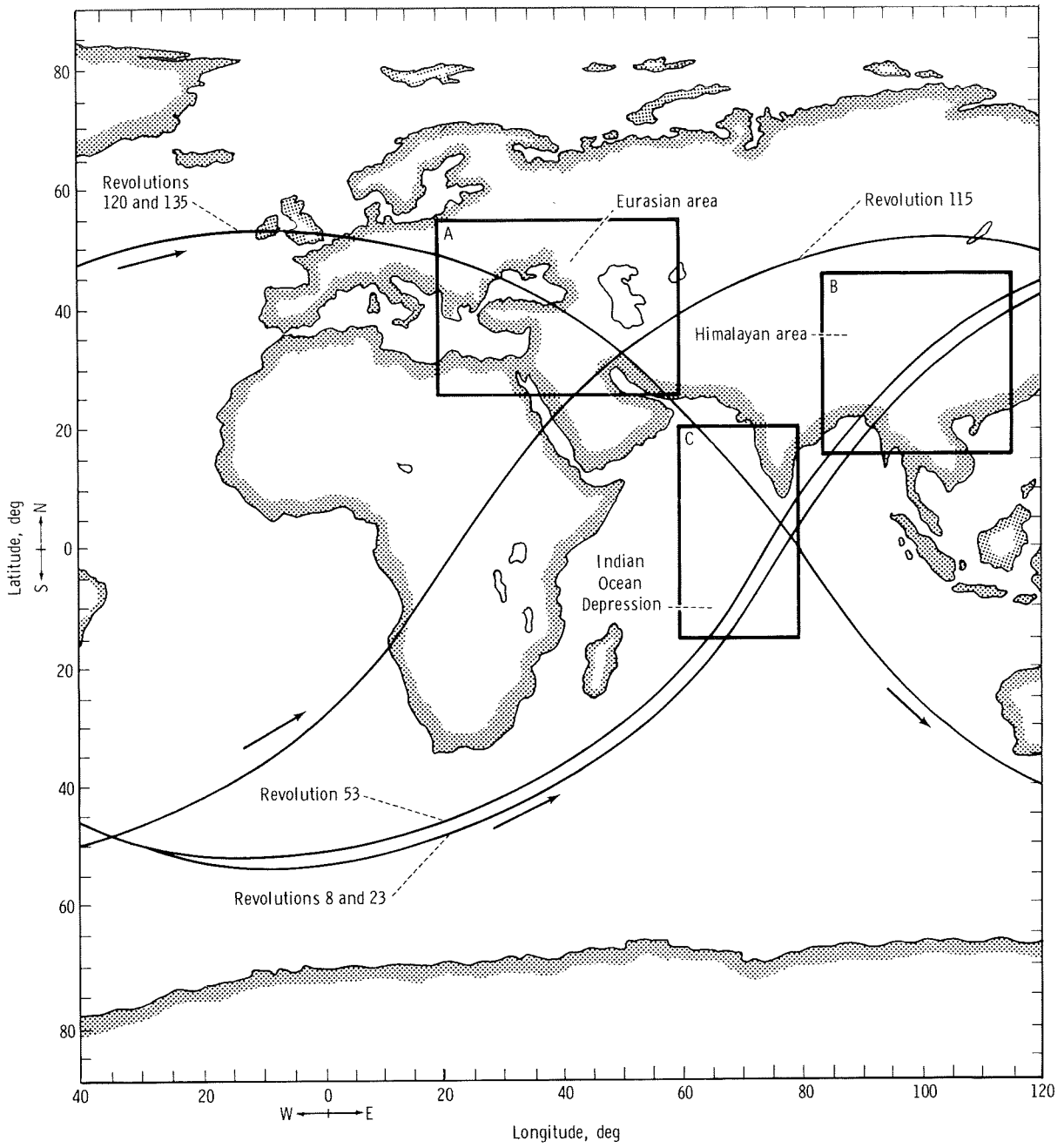

FIGURE 11-8.—Apollo spacecraft groundtracks. "A" represents the Eurasian area; "B," the Himalayan area; and "C," the Indian Ocean Depression.

and African tectonic plates. One revolution (115), which was one of the targets-of-opportunity revolutions, passed over West Central Africa in a region where geoid undulations vary between ±20 m. In addition, this revolution is in the vicinity of a large magnetic anomaly, namely the Bangui Anomaly centered at approximately latitude 3° N and longitude 18° E.

Based on an analysis of the residual patterns (ref. 11-7), the location of blocks for recovery of gravity anomalies was made for each experiment revolution separately by placing the block where the residuals change sign. The parameters estimated were the orbital parameters for the Apollo spacecraft, the ATS-6 satellite orbital parameters, and the gravity anomalies. The size of each anomaly block chosen was 4° by 4°. The latter dimension for the blocks is consistent with the region of sensitivity of the Apollo spacecraft.

In the prime experiment area, i.e., the Indian Ocean Depression, three ascending and two descending revolutions were used for recovery of 4° by 4° gravity anomaly blocks in the vicinity of the geometric center of this feature. The ascending revolutions were 8, 23, and 53 and the descending revolutions were 120 and 135. Figure 11-8 shows the groundtrack of each of these revolutions, and figure 11-9 shows in detail the groundtrack and associated 4° by 4° anomalies recovered. This area was denoted in figure 11-8 as "C." In figures 11-9 and 11-10, attention is focused on the fact that blocks in similar geographic regions obtained independently from parallel passes are in excellent agreement. (See figure 11-9 for value and ground truth[2] comparison.) Closer inspection of figure 11-9 yields an even more striking result, which is that values obtained for the anomaly blocks using the aforementioned ascending and descending revolutions are of comparable values for similar geographic location. (See blocks in figure 11-9 contained in 10° by 10° block centered at latitude 0°, longitude 75° E.)

Another recovery of a consistent set of gravity anomaly magnitudes for 4° by 4° anomaly blocks was obtained during revolutions 120 and 135 (fig. 11-10). The geographic area for which the gravity anomalies were recovered corresponds to the area known as the Zagros Thrust Zone (ref. 11-8), which is at the juncture of the African and Eurasian tectonic plates.

Figures 11-5 and 11-6 contain SST range sum rate residuals both before and after the estimation of the gravity anomalies. Initially, the anomaly adjustment reduced the overall magnitude of the residuals but it does not entirely remove systematic signatures. Further analyses have shown that placement of the anomaly blocks to be estimated is "critical." Results have been obtained that lead to the conclusion that the estimate for the magnitude of anomaly blocks is within close agreement for small deviations in the placement of blocks.

The technique of fitting a cubic spline to calculate residual derivatives (i.e., accelerations), used successfully by Muller and Sjogren (ref. 11-7) for the recovery of lunar gravity anomalies, was used for this application. Eleven blocks were placed at the points along the orbit at which peak accelerations occurred. After again solving for the state vectors for the Apollo spacecraft, the ATS-6 satellite, and the magnitude of the 11 anomaly blocks, the residuals were reduced by a factor of 2. The remaining systematic pattern in the residuals appears to correlate with the spacecraft attitude control motion. This latter effect is being studied in greater detail. The residual patterns resulting from the use of this technique are shown in figure 11-5.

Revolution 115, one of the unscheduled revolutions, proved to be of great importance, both from the aspect of detectability and recoverability. During this revolution, the Apollo spacecraft passed over two anomalies in Africa. In fact, during the interval that Apollo passed over Africa, the

[2]Ground truth is obtained from a set of surface gravity data collected from multiple sources. The anomalies derived from this data set do not necessarily coincide with the recovered anomaly blocks under the Apollo orbit.

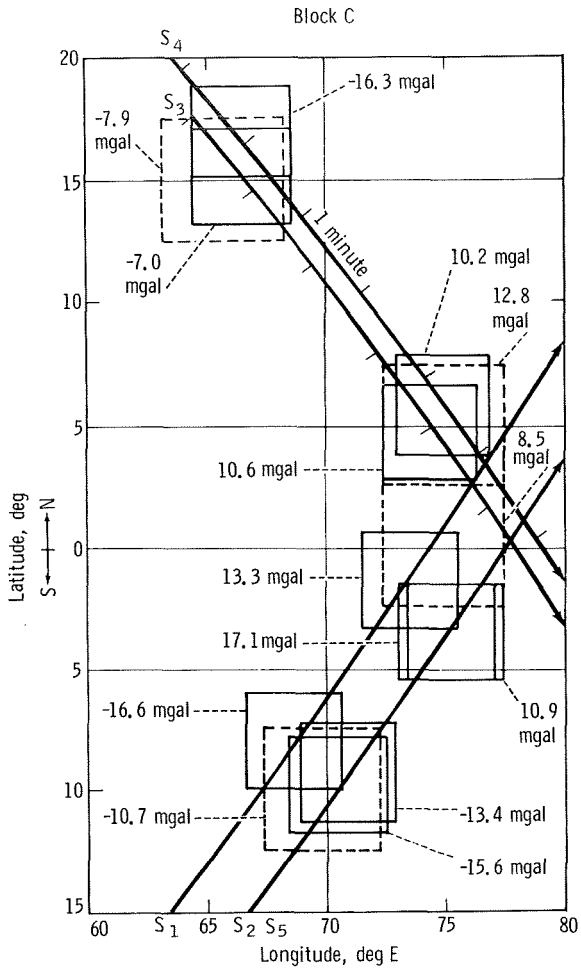

S_1 = Start time - revolution 53 = 06:23
S_2 = Start time - revolution 8 = 07:27
S_3 = Start time - revolution 135 = 15:48
S_4 = Start time - revolution 120 = 16:08
S_5 = Start time - revolution 23 = 07:01

Recovered block
Ground truth
Note: 1 gal = 0.01 m/sec^2

RECOVERED ANOMALIES

Revolution no.	Latitude, deg	Longitude, deg E	Size	Value, mgal
120	16.8	66.8	4° by 4°	-16.3
135	15.2	66.8	4° by 4°	-7.0
120	5.7	75.1	4° by 4°	10.2
135	4.6	74.6	4° by 4°	10.6
53	-1.5	73.5	4° by 4°	13.13
23	-3.5	75.0	4° by 4°	17.1
8	-3.5	75.2	4° by 4°	10.9
53	-8.0	68.8	4° by 4°	-16.6
23	-9.3	71.0	4° by 4°	-13.4
8	-9.9	70.5	4° by 4°	-15.6

Indian Ocean area

GROUND TRUTH

Latitude, deg	Longitude, deg E	Size	Value, mgal
15	66	5° by 5°	-7.9
5	75	5° by 5°	12.8
0	75	5° by 5°	8.5
-10	70	5° by 5°	-10.7

FIGURE 11-9.—Detailed groundtrack of gravity anomaly recovery for the Indian Ocean area together with recovered anomalies and ground truth. Boxed data represent the Indian Ocean area.

spacecraft was directly underneath the ATS-6 satellite. Therefore, the rate of change of the range sum rate residuals was a direct measure of the anomalous gravitational acceleration.

The residual pattern before adjusting anomaly blocks (fig. 11-7) exhibited a large residual signature allegedly due to gravity field perturbations. At this point in the analysis it was felt that a better technique for placement of anomaly blocks was needed.

SUMMARY AND CONCLUSIONS

The high/low SST technique can be utilized for Earth gravity anomaly detection. Anomalies having dimensions equal to or longer than the height

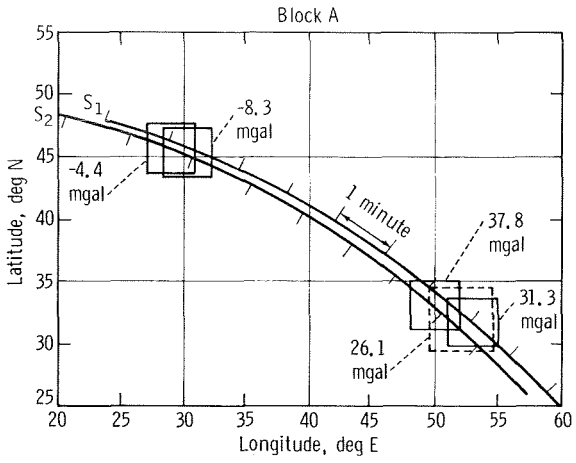

S_1 = Start time - revolution 120 = 15:57
S_2 = Start time - revolution 135 = 15:36

□ Recovered block
⬚ Ground truth
Note: 1 gal = 0.01 m/sec^2

RECOVERED ANOMALIES

Revolution no.	Latitude, deg N	Longitude, deg E	Size	Value, mgal
135	45.5	29.2	4° by 4°	-4.4
120	45.4	30.5	4° by 4°	-8.3
135	33.1	50.0	4° by 4°	37.8
120	31.7	52.9	4° by 4°	31.3

GROUND TRUTH

Latitude, deg N	Longitude, deg E	Size	Value, mgal
32	52	5° by 5°	26.1

FIGURE 11-10.—Detailed groundtrack of gravity anomaly recovery for the Eurasian area together with recovered anomalies and ground truth.

of the low spacecraft and having values of approximately 0.05 mm/sec^2 (5 mgal) have been detected with a good 10:1 signal-to-noise ratio. The 0.05-cm/sec range rate, conservatively computed before the experiment, was actually improved by the measured noise of 0.03 cm/sec. For all the passes examined, it was possible to correlate the measured range-rate residuals with known geoidal features of short wavelength (approximately 300 km). It was further demonstrated that the range-rate signatures could be repeated orbit by orbit; thus, confidence in the experiment data has been increased.

The results which have been described in this report clearly show that the ASTP Geodynamics Experiment goals have been met; that is, the high/low configuration SST technique for detectability and recoverability of gravity anomalies is successful. This technique represents another source with which the geopotential can be mapped and modeled. Thus, the entire 108 experiment revolutions collectively form a data set that is "rich" in scientific information for geodynamic investigations.

Further analyses using the Geodynamics Experiment data will range from the developing of an improved model for the geopotential to the correlating of experiment data with bathymetric features and plate tectonic boundaries within the ATS-6 visibility region of the Apollo spacecraft. Correlations will also be made with satellite-to-satellite range sum rate data and altimeter data obtained from the GEOS-3 program.

REFERENCES

11-1. Vonbun, F. O.; and Mengel, J. T.: Tracking and Communications for Planetary Manned Missions. J. Spacecraft & Rockets, vol. 5, no. 5, July 1968, pp. 863-865.

11-2. Vonbun, F. O.: The ATS-F/Nimbus-E Tracking Experiment. Rotation of the Earth, Paul Melchoir and Shigeru Yumi, eds., D. Reidel Publ. Co. (Dordrecht, Holland), 1972, pp. 112-120.

11-3. Schmid, P. E.; and Vonbun, F. O.: The ATS-F/Nimbus-F Tracking and Orbit Determination Experiment. 1974 IEEE Intercon Technical Program Papers, 1974, pp. 34/6-1 and 34/6-2.

11-4. Schwarz, Charles R.: Gravity Field Refinement by Satellite to Satellite Doppler Tracking. NASA CR-117404, 1970.

11-5. Bryan, J.: ATS-F/GEOS-C Satellite to Satellite Tracking Data Processing Consideration. NASA TM X-70736, 1974.

11-6. Lerch, Francis J.; Wagner, Carl A.; et al.: Gravitational Field Models for the Earth (GEM 1 & GEM 2). NASA TM X-65970, 1972.

11-7. Muller, P. M.; and Sjogren, W. L.: Mascons, Lunar Mass Concentrations. Science, vol. 161, no. 3482, 1968, pp. 680-684.

11-8. Lomnitz, Cinna: Global Tectonics and Earthquake Risk. Elsevier Scientific Publishing Co. (New York), 1974.